Journal Pre-proof

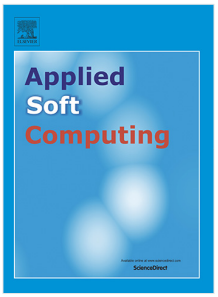

Accurate multi-class image segmentation using weak continuity constraints and neutrosophic set

Soumyadip Dhar, Malay K. Kundu

PII: S1568-4946(21)00680-3
DOI: https://doi.org/10.1016/j.asoc.2021.107759
Reference: ASOC 107759

To appear in: *Applied Soft Computing*

Received date : 22 March 2020
Revised date : 25 June 2021
Accepted date : 27 July 2021

Please cite this article as: S. Dhar and M.K. Kundu, Accurate multi-class image segmentation using weak continuity constraints and neutrosophic set, *Applied Soft Computing* (2021), doi: https://doi.org/10.1016/j.asoc.2021.107759.

Accurate multi-class image segmentation using weak continuity constraints and neutrosophic set

Soumyadip Dhar[a], Malay K. Kundu[b]

[a]*RCCIIT,Kolkata-*700015,*India, rccsoumya@gmail.com*
[b]*ISI,Kolkata-*700108,*India, malay@isical.ac.in*

Abstract

In this paper, we propose a multi-class image segmentation method based on uncertainty management by weak continuity constraints and neutrosophic set (NS).To manage the uncertainties in the segmentation process, an image is mapped into the NS domain. In the NS domain, the image is represented as true, false, and indeterminate subsets. In the proposed method, accurate segmentation is achieved by minimizing an energy function in the NS domain. The theory of weak continuity constraints is integrated into the NS domain to generate the energy function. The weak continuity constraints take into account the spatial and boundary information of the segments to manage the uncertainties in the segmentation process. The proposed method can automatically segment an image iteratively without any prior knowledge about the number of classes. The performance of the proposed method is compared with state-of-the-art methods and it is found to be quite satisfactory. The proposed method's performance under noise perturbations is statistically validated using a modified Cramer-Rao bound. The bound predicts the performance of image segmentation algorithms and serves as a benchmark for segmentation results.

Keywords: *Image segmentation* , *Uncertainty management*, *Weak continuity constraints*, *Neutrosophic set*, *Energy function*

1. Introduction

The modern age is the age of automation. In this modern era, there is a lot of applications of image processing in metal industries [1], agriculture industries [2], robotics [3], and medical sciences [4]. The application varies from automatic fault detection, quality detection to MRI and CT scan processing, etc. In various stages of image processing, image segmentation especially the segmentation of a multi-class image is one of the essential task [5]. In the multi-class image segmentation process, an image is segmented into different regions based on different features. For proper segmentation, the variations among the pixels in the same segment should be decreased with the increase in the variation among different segments. Moreover, an efficient segmentation technique should also be able to determine the boundaries between the segments accurately. The localization of the segment boundaries with the detection of segments is an ill-posed problem [6]. This is due to the uncertainties involved in the process of segmentation [7]. The automatic detection of the number of segments in an image without having any predefined knowledge is also a difficult task. As both of these problems emerge in highly uncertain image patterns, they must be addressed properly for an efficient segmentation algorithm to be developed.

1.1. Related works

The literature on different types of segmentation techniques is quite rich. Currently, the segmentation techniques based on the edge, graph, region, and energy are quite popular. Zhang et al. [8] proposed a graph-based technique for fast image segmentation. Here, an image was segmented based on the partitioning of the graph. In the paper, Bragantini et al. [9] extended the concept of Image Foresting Transform (IFT) for the graph-based classification of different objects in an image. The graph-based dominant set concept was utilized by Mequanint et al. [10] for the segmentation of an image into different classes. Niu et al. [11] proposed a region-based method based on local similarity for the segmentation of regions in an image. The method required no pre-processing and thus preserved the image structure accurately. Edge or contour-based methods were used by the authors in [12, 13]. In the edge-based methods, the gradient was utilized to generate the proper segments. Among all the conventional methods, segmentations based on thresholding are very popular due to the simplicity of the techniques. Multilevel thresholding based on Tsallis-Havrda-Charvat entropy was proposed by Borjigin et al. [14]. Upadhyay et al. [15] proposed multilevel image thresholding using Kapur's entropy. Several unconventional techniques were also utilized by some researchers for the segmentation of an image. Algebraic topology-based image segmentation was proposed by Assaf et al. [16]. A persistent homology technique of algebraic topology was utilized here for the segmentation purpose. Wang et al. [17] presented a geometric flow-based bandlet transform for segmentation. The particle replanting algorithm was employed here to deal with the region merging or separating in an image.

The methods mentioned above gave no attention to manage the uncertainties that arise in the segmentation process. Thus, the methods were less tolerant of the ambiguities due to complex image patterns, different types of perturbations etc [18].

In the literature on segmentation, a lot of methods used uncertainty handing techniques for the accurate classification of regions in an image. They mainly used fuzzy set [19, 20, 21], rough set [22] or neutrosophic set [23] for uncertainty handling. In the paper [24] we proposed a type-2 fuzzy set-based multi-class image segmentation. Out of the three sets, the neutrosophic set (NS) is relatively new and it is very popular to handle various types of uncertainties. The applications of NS in the field of image segmentation were found to be quite effective [25, 26].

Due to high computational complexity in multi-class image segmentation, several researchers used different meta-heuristic search algorithms to compute the thresholds. In the paper proposed by Li et al. [27] authors used fuzzy coyote optimization algorithm for multi-class segmentation. They used Otsu and fuzzy entropy as their objective functions. They did not consider the boundary information between the regions of an image. Wunnava et al. [28] proposed an adaptive Harris hawks optimization method for multi-class image segmentation. Multi-level thresholding by minimizing Tsallis fuzzy entropy was proposed by Raj et al. [29]. Here they utilized a differential evolution algorithm to search the thresholds. The authors in the paper [30] investigated butterfly optimization and gases Brownian motion optimization for multi-class segmentation. Bat algorithm and type-2 fuzzy-based image segmentation was proposed by us in the paper [31]. The limitation of the

meta-heuristic search-based algorithms is that, in most cases, they are not fully automatic. That means, the number of the thresholds should be pre-defined. Moreover, a large number of parameters should be initialized in those algorithms.

One ideal segmentation technique should have some important properties. The technique should consider the spatial information along with the gray level information for capturing the texture of a segment. The method should also consider the boundary information with the utilization of some proper uncertainty handling tools.

1.2. Proposed method and novelty of the method

Some of the methods found in the literature incorporate local information for segmentation [14, 32]. But the methods have no provision for capturing the boundary information between the segments. Moreover, in most of the methods, the number of classes or segments are ad-hoc or fixed. That means they should have prior knowledge about the number of segments in an image. Additionally, the conventional methods, which do not have any uncertainties handling tools could not reduce the ambiguities in an image. These limitations restrict the methods to reach the highest level of accuracy and they also leave room for improvement of the methods for practical applications.

Because of the above limitations, we propose an automatic multi-class image segmentation method based on weak continuity constraints. The weak continuity constraints help to localize the boundaries between the segments in the image. It also takes into account local or spatial information during segmentation. In the field of computer vision, weak continuity constraints were efficiently used for image reconstruction [33, 34]. Weak continuity con-

straints in a set of data are the constraints that can be violated but with a penalty. The property is used to localize the discontinuities in a set of reconstructed values. One can find in [34] that weak continuity constraints are powerful tools for discontinuity detection. Conventional methods for discontinuity detection blur the original signal. No such problem arises in weak continuity constraints and they detect the discontinuities robustly and accurately without any prior information about the position of discontinuities. The boundaries between the classes in a segmented image may not be strong due to low-intensity change, i.e low gradient at the boundary area between the two classes. This may increase the uncertainties in the segmentation process. Thresholding depending only on the intensity values of the pixels may disconnect the weak boundaries. The thresholding using weak continuity constraints helps to localize the segmentation boundaries, and thus it is useful for uncertainty management.

As already mentioned recently, we have proposed a segmentation method using weak continuity constraints in the type-2 fuzzy set domain [24] with high accuracy. But, the limitation of a type-2 fuzzy set is that it requires a type-reduction, which has high computational complexity. Given the above limitations, in this paper, we propose weak continuity constraints-based segmentation in the NS domain.

To manage the uncertainties in the segmentation process accurately, we apply the weak continuity constraints in the NS domain. The NS was proposed by Florentin Smarandache [23]. An NS is represented by three subsets. They are true, indeterminate, and false subsets. For an image segmentation process by NS, the image is converted into a neutrosophic image. This is

followed by the minimization of the uncertainties to generate the segments [35, 36, 37].

The novelty of the proposed method is that here we propose an energy function in the NS domain based on weak continuity constraints for image segmentation. The energy function acts as an objective function for segmentation in the NS domain. The objective function can express the gray level and spatial ambiguity in an image in the NS domain and the minimization of the function minimizes the ambiguities. The proposed method automatically determines the segments iteratively in an image without any prior knowledge. The iteration stops when a proposed base condition is satisfied. The schematic diagram of the proposed method is shown in Figure 1.

We have already mentioned that we incorporated the weak continuity constraints in the fuzzy set domain for segmentation [24, 21]. In image segmentation using a fuzzy set, one pixel can have different membership for representing the belongingness of the pixel into different classes. But, it has no provision for representing the portion in between the classes explicitly. Logically, the portion should be represented separately by another set. In NS, the set is called an indeterminate subset. Thus, the representation of an image into an NS domain is significantly different from the representation of the image into fuzzy domain. In this paper, we incorporate the weak continuity constraints in the NS domain for automatic multi-class segmentation. We use the indeterminate subset of the NS for boundary regions and the true subset of the NS for non-boundary regions. It is expected that the two subset representation of NS will give better performance than that of the conventional fuzzy set in the segmentation process.

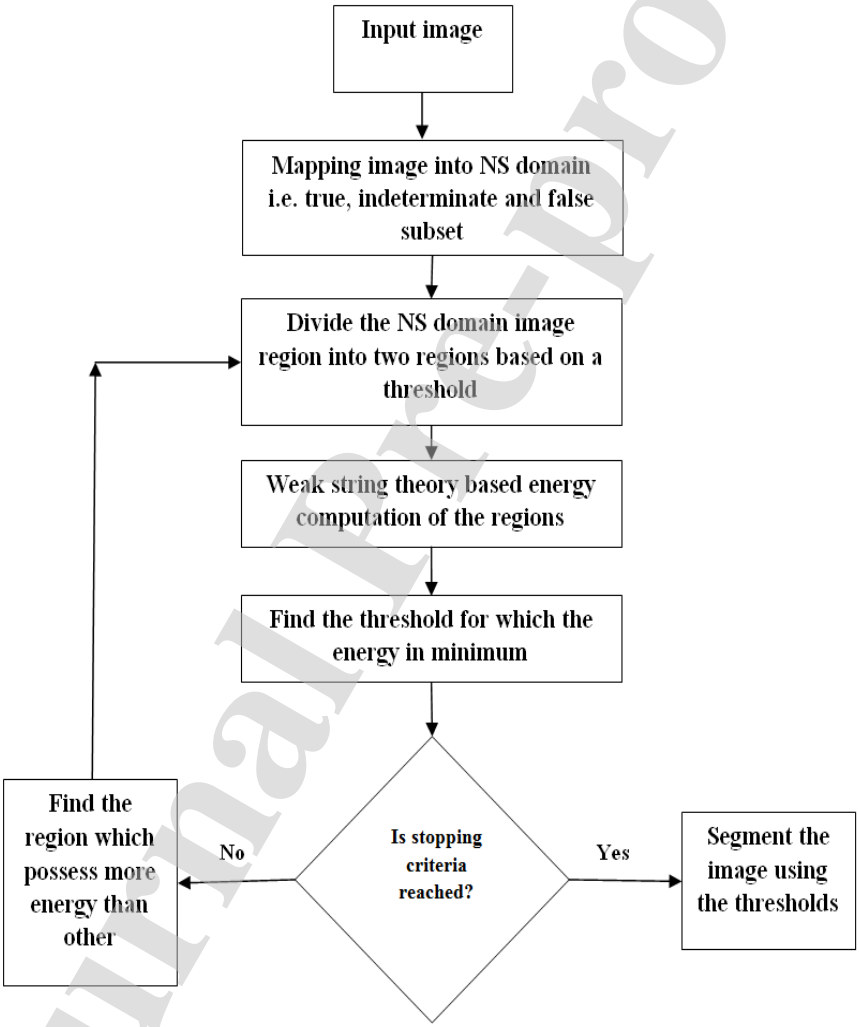

Figure 1: Schematic diagram of the proposed method

The rest of the paper is as follows: The brief introduction of the neutrosophic set (NS), mapping of an image into the NS domain, the theory of weak continuity constraints, the application of the weak continuity constraints in the NS domain for segmentation, and proposed algorithm are described in Section 2. The results are discussed in Section 3. The section includes different quantitative measures, comparison with the other methods on different datasets, and statistical validation by modified Cramer-Rao bound.

2. Segmentation based on neutrosophic set with weak continuity constraints

2.1. Neutrosophic set

Let A be a neutrosophic set (NS). An element x from the union of discourse U will belong to A as $x(T, I, F)$. It means that the belongingness of x to true subset T is $t\%$, indeterminate subset I is $i\%$ and false subset F is $f\%$. T,I and F represents the standard or non-standard subsets, which have the open interval represented by $]^{-}0, 1^{+}[$. The elements of T,I and F can have any value between [0 1]. For practical use it is assumed $T, I, F \subset [0\ 1]$ with $t + f = 1$ and $i \in [0\ 1]$. Details theory about NS can be found in [23].

2.2. Mapping of an image into neutrosophic domain

An image in the NS domain is called a neutrosophic image (NI). Let us consider an L level image R of dimensions $P \times Q$ where $R(i, j)$ represents the intensity of a pixel at the position (i, j): $i = 1, 2, .., \mathrm{P}$, $j = 1, 2, ...\mathrm{Q}$. The neutrosophic image is given by three subsets: T,I and F. In a neutrosophic image, a pixel belongs to the three subsets and they are represented as $T(i, j)$,

$I(i,j)$ and $F(i,j)$. The mapping of the image into the NS domain is given by the following equations [38].

$$T(i,j) = 1 - \frac{\overline{R}_{max} - \overline{R}(i,j)}{\overline{R}_{max} - \overline{R}_{min}} \tag{1}$$

$$I(i,j) = 1 - \frac{d_{max} - d(i,j)}{d_{max} - d_{min}} \tag{2}$$

$$d(i,j) = \text{abs}(R(i,j) - \overline{R}(i,j)) \tag{3}$$

$$d_{\max} = \max\{d(i,j) | i \in \text{P}, j \in \text{Q}\} \tag{4}$$

$$d_{\min} = \min\{d(i,j) | i \in \text{P}, j \in \text{Q}\} \tag{5}$$

$$F(i,j) = 1 - T(i,j) \tag{6}$$

Here, $\overline{R}(i,j)$ is calculated by taking the mean of the pixel intensities within a local neighborhood of dimensions with the window size $w \times w$. The $\overline{R}(i,j)$ is placed at the mid-position of the window. The window size $w \times w$ for mapping an image into the NS domain in the proposed method is taken as 7×7. The value of $I(i,j)$ is utilized to calculate the degree of indeterminacy of a pixel, which represents the uncertainties in deciding the brightness of a pixel. The contrast in the image is increased in the NS domain by $\alpha - mean$ and $\beta - enhancement$ operations [39]. These two operations make the image

more effective for the process of segmentation.

2.3. Multi-thresholding in NS domain

In the proposed method, the multi-class segmentation is achieved by multi-thresholding. In a thresholding process, if a pixel x is less than the threshold t i.e $x < t$, then x belongs to the background region. Again, if a pixel x is greater than or equal to t i.e $x \geq t$, then the pixel belongs to the object region. In an NI, the corresponding element of x is given by x_{NI}. That means $x_{NI}(i, j)$ represents the NI image value of $x(i, j)$.

In the NS domain, the total entropy of the subsets is used to measure the uncertainties in the segmentation process. But the measure does not take into consideration the neighborhood information of the boundary points between the classes. So, the measure may be biased towards the high or low value of the subsets and it has no separate provision to introduce the boundary information in the entropy measure. To circumvent the problem, we introduce the concept of weak continuity constraints in the segmentation process. In the next section, we will discuss the weak continuity constraints.

2.4. Incorporation of weak continuity constraints in NS domain

We will describe the incorporation of weak continuity constraints in the NS domain in this subsection. First, we'll go over the theory of weak continuity constraints.

2.4.1. String under weak continuity constraints

Most of the problems in computer vision can be treated as optimization problems. For example, segmentation, edge detection, surface reconstruction,

etc. can be converted into an optimization problem. The limitation of a conventional optimization function is that there is no provision to treat the discontinuities explicitly. But the knowledge of discontinuity is essential for the proper solution of different problems in computer vision. The knowledge can be incorporated with the help of weak continuity constraints. In weak continuity constraints, for a set of values, the constraints can be violated at a cost. Thus, a penalty term comes into play with the violation of continuity constraints and it helps to localize the point of discontinuities in the weak region. Due to this unique property, the concept is used in computer vision techniques for localization of discontinuities or edges [33, 34]. For the NS-based segmentation using weak continuity constraints, we embrace the theory of weak elastic string under weak continuity constraints.

In computer vision, string theory is used for the visual reconstruction of data [33]. In the visual reconstruction, the objective is to interpolate a data $d_s(x)$ to a data $u_s(x)$ in a string such that the energy of the string is minimum. In doing so the string may be broken at the point of weak continuities and the discontinuities are localized. The characteristic of the string is expressed by the energy of the string. The energy is the sum of three parts that define the string. They are the measure of faithfulness D_s, stretching energy S_s and penalty P_s. Mathematically, the three components are written as

$$\begin{aligned} D_s &= \int_0^N (u_s - d_s)^2 dx \\ S_s &= \lambda_s^2 \int_0^N (u_s')^2 dx \end{aligned} \tag{7}$$

The P_s represents the total penalty with a constant penalty parameter γ_s for each break in the string. λ_s^2 is the measure of elasticity of the string. For the reconstruction process λ_s is a scale constant [33]. The objective is to minimize the energy $E_s = D_s + S_s + P_s$. In the discrete form, the string energy is expressed as follows

$$\begin{aligned} \text{Measure of faithfulness } D_s &= \sum_{i=1}^{N} (u_{s_i} - d_{s_i})^2 \\ \text{Stretching energy } S_s &= \lambda_s^2 \sum_{i=1}^{N-1} (u_{s_i} - u_{s_{i+1}})^2 (1 - l_{s_i}) \\ \text{Penalty } P_s &= \gamma_s \sum_{i=1}^{N-1} l_{s_i} \end{aligned} \tag{8}$$

Here l_{s_i} is the boolean variable and it is 1 at the point of discontinuities and otherwise it is 0.

2.4.2. Weak continuity based proposed energy function in NS domain for segmentation

In the process of image segmentation, an image is divided into a set of disjoint classes. Thus, it can be said that it is a mapping process in which each pixel of an image R is mapped into one class. The mapping function $f : R \rightarrow Rg$ where Rg denotes the group of all pixels and Rg_1, Rg_2....Rg_c are the c segments then $Rg = Rg_1 \bigcup Rg_2 \bigcup .... \bigcup Rg_c$ such that $Rg_i \bigcap Rg_j = \phi$ where $i \neq j$ and $i, j \in [1 \quad c]$. The segment i is represented by a prototype (e.g segment center) $v(Rg_i)$. The pixel values are either constant or vary very slowly, i.e they are almost continuous within a segment Rg_i. The variation of the pixel values would be high at the boundary between the two segments.

The boundary is the location of the discontinuity between the segments. Thus, the Rg_i is continuous at every point except at the boundaries where the weak continuity constraints would be violated. Thus, it can be said that the segmentation process interpolates each pixel into different segments by $v(Rg_i)$ and the boundaries between the two segments are the point of discontinuities where the pixel values change significantly. So, the segmentation process can be expressed by an energy function in the NS domain. The energy function E_{NI} which can associate the knowledge of discontinuities in the segmentation process is defined by

$$E_{NI} = D_{NI} + S_{NI} + P_{NI} \tag{9}$$

$$D_{NI} = \sum_{i=1}^{c} \sum_{x \in Rg_i} (x - v(Rg_i))^2$$

$$S_{NI} = \lambda^2 \sum_{i=1}^{c} \sum_{x \in Rg_i} \sum_{y \in N_x} (x_{NI} - y_{NI})^2 (1 - l(x))$$

$$P_{NI} = \gamma \sum_{i=1}^{c} \sum_{x \in Rg_i} l(x) \tag{10}$$

In the above equation $v(Rg_i)$ is the segment center of Rg_i and it can be written as

$$v(Rg_i) = \frac{\sum_{x \in Rg_i} x_{NI}.x}{\sum_{x \in Rg_i} x_{NI}} \tag{11}$$

where $x_{NI} \in T$. In the above equation, $y \in N_x$ represents the set of neighborhood pixels of x within a local window of size $\lambda \times \lambda$. At the boundary points between two segments $l(x) = 1$ and at the non-boundary points $l(x) = 0$. In Eq.(10) the parameters λ, γ, $l(x)$ are analogous to the scale parameter λ_s, the penalty parameter γ_s and the boolean variable l_{s_i} of the weak string.

The accurate segmentation of an image is obtained by minimizing E_{NI} i.e the total energy generated by the true subset.

2.4.3. Representation of uncertainties by the energy function in NS domain

In this section, we discuss the representation of uncertainties by the three components D_{NI}, S_{NI}, and P_{NI} of the weak continuity constraints in the NS domain. To determine the parameters λ and γ in Eq.(10) we use the indeterminate subset of NI.

Here, D_{NI} represents the sum of the distance of the pixels values from the segment center. As already discussed, the segment center of Rg_i is given by $v(Rg_i)$ and D_{NI} signifies the difference between the pixel values and the segment prototype in which they belong.

For calculating S_{NI} the sum of the distance of the center pixel from the neighborhood pixels in the window of size $\lambda \times \lambda$ is computed. The window size $\lambda \times \lambda$ is computed based on the indeterminate subset I. There exists a tradeoff between the high value and small value of λ. The small value of λ is unable to represent the texture information properly. On the other hand, a high value of λ may blend the properties of the two segments. This situation may increase the uncertainties in the segmentation process. To find the proper size of λ we utilize the idea of spectral flatness measure (SFM) [40]. The SFM of the indeterminate subset is computed. The SFM closes to 1 signifies the image contains a lot of edges and the λ should have a low value. Again, λ should have a high value when SFM is closed to 0. In the proposed method, if $SFM > 0.5$, then $\lambda = 5$ and if $SFM \leq 0.5$, then $\lambda = 9$.

In the segmentation process, the term P_{NI} is related to the localization of the discontinuities between the segments. In the segmentation process

using thresholding, the neighborhood points (x, y) where $(x \leq t \& y > t)$ or $(x > t \& y \leq t)$ are the points of discontinuity where the weak continuity constraints should be violated. The violations of the continuity constraints come with a penalty γ. In the proposed method, if the indeterminacy I at the boundary points is high, γ is taken low. The reason is that the high value of indeterminacy means there is a high chance of the presence of boundaries between the different segments. In this scenario, the low value of γ keeps the penalty low to make the total energy low and the discontinuities are localized at the boundary points. In the same line of logic, γ is taken high when the value of indeterminacy in the boundary regions is low. In the proposed method, the γ is taken as

$$\gamma = \frac{1}{I(x) + 1} \tag{12}$$

where $I(x)$ is the value of indeterminacy at x in the indeterminate subset.

Here, the management of the uncertainties means the reduction of energy by reducing the D_{NI}, S_{NI}, and P_{NI}. To show that the reduction of energy reduces the uncertainties, we prove the following statements.

(1) *In the segmentation process, the term D_{NI} represents the gray level ambiguity in NS domain.*

Proof: The gray level ambiguity signifies the difficulty in deciding whether a gray level belongs to a particular segment of pixels or not. The ambiguity will be minimum if the pixels belong to the right segment. That means for minimum ambiguity, the distance of a pixel should be minimum from the segment prototype to which it belongs. Thus, it is obvious that D_{NI} represents the gray level ambiguity in the NS domain. Minimization of this term minimizes the uncertainties due to the gray level ambiguity.

(2) *The term $S_{NI} + P_{NI}$ represents the spatial ambiguity in NS domain.*
Proof: In the segmentation process, spatial ambiguity represents the difficulty in deciding the spatial properties of a segment. In the proposed energy function, S_{NI} measures the change of intensity values within a scale of λ. The term S_{NI} signifies the change of NI pixels values over a local neighborhood in non-boundary pixels. Within a proper class, the value of S_{NI} should be minimum since in a proper segment the pixels are the most uniform i.e $S_{NI} \to 0$. On the other hand, P_{NI} signifies the spatial information at the boundary between the segments. The penalty will be minimized if the proper boundary is detected at x with a high indeterminate value $I(x)$. Thus, the term $S_{NI} + P_{NI}$ represents the spatial ambiguity of an image, and minimization of $S_{NI} + P_{NI}$ minimizes the ambiguity.

From the above discussion, it is clear that the minimization of the energy E_{NI} minimizes the gray level and spatial ambiguities in an image. Thus, the uncertainties in the segmentation are managed by the reduction of energy. Moreover, the weak continuity constraints help to localize the discontinuities in a string. So, from the segmentation point of view, the inclusion of weak continuity constraints in the pixel values of the NI helps to localize the segmentation boundaries accurately. In the proposed method, the energy function E_{NI} acts as an objective function for the image segmentation and the purpose of the proposed method is to minimize the objective function to generate the accurate segments by managing the uncertainties. Next, we prove the following theorem.

Theorem 1: The accurate threshold t produces minimum energy E_{NI} in the NS domain.

Proof: Let us consider t be an accurate threshold of an image $R \in [x_{min} \quad x_{max}]$. Let us assume that the threshold t will generate the segments Rg_1 and Rg_2 in the image. Let t' be another threshold in R and $t \neq t'$. Let Rg_1' and Rg_2' are the two segments generated by t'. Since, t is an accurate threshold the NS true value (i.e T) of the segments Rg_1 and Rg_2 are almost uniform. That means $x \approx y, \forall (x,y) \in T_{Rg_1}$, and $x \approx y, \forall (x,y) \in T_{Rg_2}$. Here, T_{Rg_1} and T_{Rg_2} represent true values of the regions Rg_1 and Rg_2 respectively. But, for the threshold t' we can find $\exists (x,y) \in T_{Rg_1'}$ such that $x \neq y$. Similarly, we can find $\exists (x,y) \in T_{Rg_2'}$ such that $x \neq y$. So, the gray level ambiguity is lower if we choose the threshold t. So, we can write $D_{NI_t} < D_{NI_{t'}}$ from Eq.(10). Here, D_{NI_t} and $D_{NI_{t'}}$ represents D_{NI} due to t and t' respectively. Similarly, since the neighborhood pixel true values are almost uniform, if t is chosen, we can say $S_{NI_t} < S_{NI_{t'}}$ from Eq.(10). Now, as t' will detect the false boundary, as per the theory of weak continuity constraints, the penalty would be more if we choose t' as a threshold point. So, we can write $P_{NI_t} < P_{NI_{t'}}$. So, we can say $D_t + S_{NI_t} + P_{NI_t} < D_{NI_{t'}} + S_{NI_{t'}} + P_{NI_{t'}} \Rightarrow E_{NI_t} < E_{NI_{t'}}$. Hence the proof.

In the next subsection we present the algorithm for multi-class image segmentation.

2.5. Proposed iterative algorithm for segmentation

In the proposed method, no prior knowledge about the number of classes is used for the segmentation. The number of classes is determined automatically using an iterative scheme. In the process, first, the image $R = [x_{min} \quad x_{max}]$ is transformed into NI. It is followed by the determination of background set $R_b = [x_{min} \quad t]$ and object set $R_o = [t+1 \quad x_{max}]$ with the en-

ergies E_{NI_b} and E_{NI_o} respectively in the NS domain depending on a threshold $t \in [x_{min} \quad x_{max}]$. The threshold t for which the energy $E_{NI} = E_{NI_b} + E_{NI_o}$ is minimum is the correct threshold which segments the image into object and background accurately. Then the set which possesses more energy than the other (i.e either $E_{NI_b} > E_{NI_o}$ or $E_{NI_o} > E_{NI_b}$) is again divided into two subsets. The process is repeated iteratively until a stopping criterion is satisfied. That means a tree structure is generated until a stopping criterion is satisfied. The stopping criterion is based on segmentation index (CI_K) for a set of segments $K = \{Rg_1, Rg_2, ..., Rg_c\}$ and it is defined as

$$CI_K = \frac{\sum_{i=1}^{c} E_{NI_{Rg_i}}}{var(v(Rg_1), v(Rg_2), ..., v(Rg_c))} \tag{13}$$

In the above equation, $E_{NI_{R_i}}$ is the energy of a segment Rg_i and $var(.)$ is the variance. From the theory of weak continuity constraints for a proper set of classes, the total energy should be low. Again from the segmentation point of view the total variation among the segment centers $v(Rg_i)$'s should be high. In the above equation, the segment centers are determined from the true subset T by Eq.(11). That means for a proper set of segments, the CI_K should be as low as possible. The iterative process will stop at ith level when $CI_{K_{i-1}} > CI_{K_i} < CI_{K_{i+1}}$ where K_{i-1}, K_i and K_{i+1} represent the set of segments at $(i-1)$th, ith and $(i+1)$th level of the generated tree. The proposed method is shown in Algorithm 1.

Figure 2 shows the segmentation process of an image R containing three regions. They are circular (Rg_2), triangular (Rg_4) and background (Rg_3) regions. At first the image is divided into Rg_1 and Rg_2 regions. Let us assume

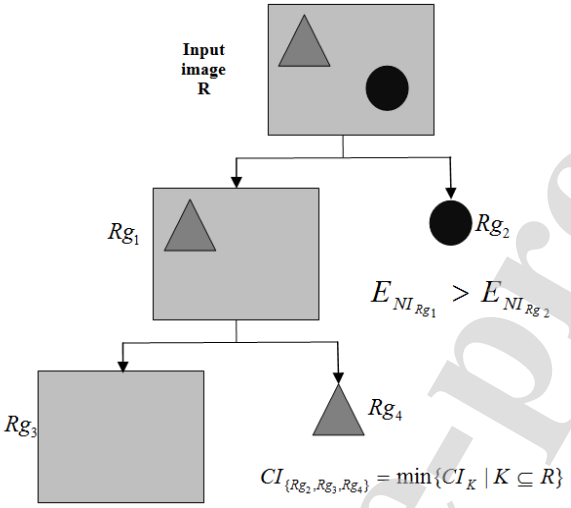

Figure 2: Iterative segmentation of an image

that $E_{NI_{Rg_1}} > E_{NI_{Rg_2}}$. Thus, the region Rg_1 is again divided into the regions Rg_3 and Rg_4. The iteration stops here because the segmentation index of $\{Rg_2, Rg_3, Rg_4\}$ given by $CI_{\{Rg_2,Rg_3,Rg_4\}}$ is the minimum among all the subsets K in R.

2.6. Computational complexity

The computational complexity (worst case) of the proposed method is given as follows. Let us assume the image contains n pixels and the image can be divided into c segments. Thus, the computational complexity of the proposed method is given by $O(cn^2)$.

3. Results and discussion

In this section, we discuss the performance of the proposed method on different datasets. For this, at first in the next subsection, we describe dif-

ferent performance measures and a technique for statistical validation using modified Cramer-Rao bound.

3.1. Performance measures and statistical validation

In this section, we will first describe different quantitative measures followed by statistical validation using modified Cramer-Rao bound.

3.1.1. Quantitative measures

For measuring the performance of the proposed method quantitatively, we used four measures. The measures are Segmentation Accuracy (SA) [41], Rand index (RI) [42], Global Consistency Error (GCE) [42] and Fuzzy evaluation (FE) [43]. The SA measures the correctly classified pixels with respect to the total number of pixels. Higher SA indicates better segmentation results. The SA is given by

$$SA = \sum_{i}^{c} \frac{A_i \cup C_i}{\sum_{j=1}^{c} C_i} \tag{14}$$

Here, A_i represents the ith class found by the algorithm and C_i represents the ith class given by the ground truth and n is the total number of pixels. The RI index tends to 1 when the segmented image is close to the ground truth. The RI index tends to 0 means poor performance by the method. Mathematically, the RI is given by

$$RI = 1 - \frac{a+b}{n(n-1)/2} \tag{15}$$

where a is the number of the pixels that belong to the same segment in segmentation result and ground truth, and b is the number of the pixels in the

different regions in segmentation result and ground truth. The GCE represents the similarities between the segmented image with the corresponding ground truth. The consistency is measured by how similar regions are assigned to similar segments in both results (segmentation result and ground truth). It varies between 0 and 1. GCE closes to 0 when the segmented image is similar to ground-truth.

All the measures described above indicate the performance of an unsupervised segmentation method. But, due to the subjective nature of the image segmentation, it is difficult to measure the performances of the methods using the crisp techniques described above. To minimize the difficulty, we also used fuzzy-based evaluation techniques proposed by the authors in [43]. In this technique, a fuzzy-based $F-score$ is used to evaluate the performance of a segmentation method. The FE is the $F-score$ in the fuzzy domain. The $F-score$ in the fuzzy domain is given by

$$F-score = \frac{2 \times Pr \times Re}{Pr + Re} \tag{16}$$

Here, Pr and Re represent the fuzzy precision and fuzzy recall of a segmentation result. The details about the two measures can be found in [43].

3.1.2. Statistical validation using modified Cramer-Rao bound

In the previous subsection, we have described some methods used for segmentation evaluation. But, one can not overlook the fact that the segmentation performance of a method depends on the image at hand [44]. Thus, the segmentation output may vary extensively depending on the image content.

Input: The gray level image $R = [x_{min} \quad x_{max}]$.
Output: Multi-class segmentation by a set of thresholds Th.
Initialisation : $Th = \{\phi\}$ $flag = 0$, $CI_{old} = 0$ $x_{min} = min\{x|x \in R\}$,$x_{max} = max\{x|x \in R\}$.

1: Map the image into NS domain to generate NI made by the Eq.(1)-Eq.(6). Initialize λ by SFM of indeterminate subset I.
2: **for** $t = x_{min}$ to x_{max} **do**
3: Find the segment center $v(R_b)$ for background $R_b = [x_{min} \quad t]$ using Eq.(11). Similarly, find $v(R_o)$ for object $R_o = [t+1 \quad x_{max}]$ in the NS domain by Eq.(11).
4: Calculate γ for boundary regions using the Eq.(12) and indeterminate subset I.
5: Evaluate the energies E_{NI_b}, E_{NI_o} by the terms D_{NI} S_{NI} and P_{NI} for object and background using the parameters λ and γ and True subset T and Indeterminate subset I.
6: Find $E_{NI} = E_{NI_b} + E_{NI_o}$
7: **end for**
8: Find t for which E_{NI} is minimum.
9: Compute $Th = Th \bigcup \{t\}$, $CI_{current}$, *current* being the set of segments at current level.
10: **if** $flag = 0$ **then**
11: $CI_{old} = CI_{current} + 1$, $flag = 1$
12: **end if**
13: **if** $(CI_{current} < CI_{old})$ **then**
14: $CI_{old} = CI_{current}$
15: **else**
16: Goto END.
17: **end if**
18: **if** $(E_{R_b} > E_{R_o})$ **then**
19: Put $x_{max} = t$ and go to step 2.
20: **else**
21: Put $x_{min} = t + 1$ and go to step 2.
22: **end if**
23: END: Segment the image by the thresholds Th.

Algorithm 1: Proposed algorithm for automatic multi-class segmentation by multi-thresholding.

So, it is logical to bound the performance of a method for a particular image. Peng et al. [45] proposed modified Cramer-Rao bound (mCRB) to find the maximum achievable performance of a segmentation method on an individual image. The performance was based on the mean square error (MSE) between the ground truth and the segmentation result. In the proposed method we use the lower mCRB to bound the performances. The lower bound indicates the minimum MSE achievable by any segmentation technique. The difference between the lower bound and the MSE of a method on an individual image indicates the space for improvement of the method on the image.

3.2. Performance measures using different datasets and comparison

In this section, we measured the performance of the proposed method on different test images. The test images include synthetic images [46], non-destructive testing (NDT) images from [47] and Kaggle 2018 Data Science Bowl dataset from [48]. The non-destructive testing (NDT) technique is used by industries for fault detection. The Kaggle dataset is useful for research biologists. To measure the efficiency of the proposed we also applied the method on natural images from Weizmann [49]. The size of the images varies from 200×200 to 500×500. We compared the performances of the proposed method with a fuzzy-based method by Bustince et al. [19], an energy-based method Wang et al. [50], NS based methods by Guo et al. [51], Jha et al. [52] and Multi-thresholding based method by Upadhyay et al. [15]. In this paper, the last three methods in [51], [15] and [52] are identified as method M1, method M2, and method M3 respectively. The purpose of using the different NS-based methods was to verify the claim by us that the proposed method of segmentation has better uncertainty management capacity than that of

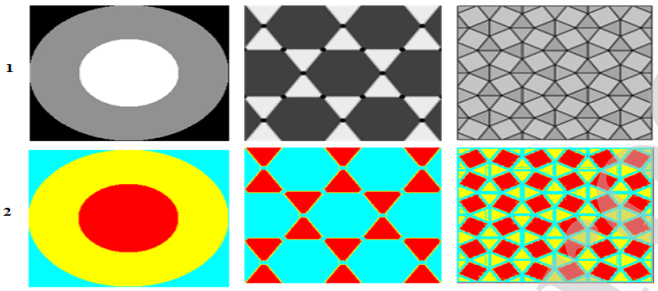

Figure 3: Row wise(1) Set of synthetic test images (2) Segmentation results by the proposed method.

the other methods in the NS domain.

3.2.1. Results on synthetic images

In this subsection, we applied the proposed method to different synthetic images. The synthetic images contained different classes in them and the proposed method had no prior knowledge about that. The objective is to show that the proposed method can determine the classes automatically. It is to be noted that for the segmentation process, the proposed method only considered the pixel intensity values, and no other features were utilized for the segmentation process. The qualitative results are shown in Figure 3. In the results, the different colors represent the different segments. From the results, it can be seen that the proposed method detected the segments correctly with the proper number of segments. That means the segmentation boundaries were localized properly with the minimization of the energy. The reason is that the proposed method managed the uncertainties properly with the minimization of the NS-based energy function. Moreover, the energy was minimized only when the correct number of segments was generated iteratively.

480 *3.2.2. Results on NDT images, outdoor scene images and other natural im-*
481 *ages*

482 Segmentations on outdoor scene images are useful in various automation
483 applications. Since these images were captured outdoors, the illumination
484 conditions may vary widely. This causes high uncertainties in those images.
485 In this subsection, we show the results of the proposed method on outdoor
486 scene images from [49]. We also show the results on NDT images. In Fig-
487 ure 4 we show the performance of the proposed method on some NDT im-
488 ages. As already mentioned, the NDT technique is used by many industries
489 for fault detection. Automatic segmentation would make the job easier for
490 them. From the visual inspection, it can be said that the proposed method
491 segmented the images correctly and localized the segmentation boundaries
492 properly. The gray level and spatial ambiguities in the shown images were
493 high and the ambiguities made the images difficult for segmentation. The
494 fact is evident from the visual inspection of the images. From the figure, it
495 is evident that the histograms are either uni-modal or there is no clear valley
496 between the classes. These types of images were very difficult to segment.
497 Moreover, in those images the number of classes was unknown. The proposed
498 method almost correctly determined the number of classes automatically de-
499 pending on the measure CI_K. The weak continuity constraints in the energy
500 function helped to localize the boundaries even in the low-intensity difference
501 between the two classes. The minimization of the stretching energy S_{NI} and
502 penalty term P_{NI} reduced the spatial ambiguities and the reduction of D_{NI}
503 reduced the gray level ambiguities in the images.

504 Here we compared the proposed method with the other methods both

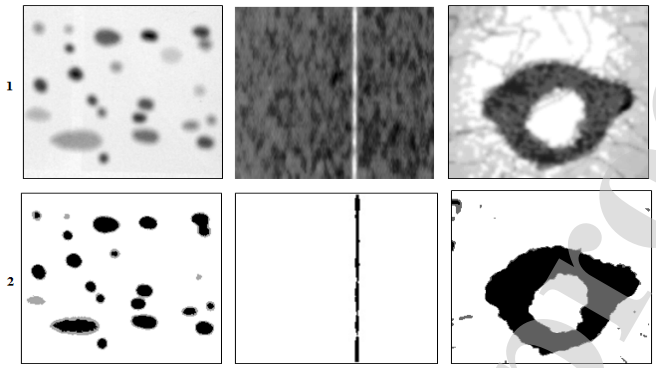

Figure 4: Row wise (1) NDT test images. (2) Segmentation results by the proposed method.

qualitatively and quantitatively on the outdoor scene images. From the results in Figure 5, we can see the qualitative performances of the methods. The quantitative performances are shown in Table 1. From the results, it can be said that the proposed method performed better than that of the other methods compared here. The method by Bustince [19] used the fuzzy-based uncertainty reduction technique for segmentation. Though the fuzzy set was a powerful tool for uncertainty reduction, the NS-based approach in the proposed method made it more suitable for managing uncertainty. The method in M1 [51] used NS-based segmentation inspired by fuzzy-c means for segmentation. The method used the concept of ambiguity segment to consider the data points at the segmentation boundaries and reduced uncertainties by reducing an objective function. But the objective function did not consider any neighborhood information and it had no provision for localization of segmentation boundaries depending on neighborhood information. The method in M3 [52] used Dice's Coefficients in the NS domain for segmentation. For this, the authors employed a filter to capture neighborhood

information. But, the filtering operation may decrease the localization accuracy by increasing the uncertainties. A Multi-thresholding based method was used in M2 [15] to segment an image. Here the researchers minimized Kapur's entropy to handle the uncertainties. In the method, the thresholds were found by the evolutionary Crow search algorithm. But, the method gave no attention to the boundaries of different segments. The method by Wang [50] used an energy-based technique for segmentation. But the method had no uncertainties handling the procedure in it.

Table 1: Quantitative performance of different methods on the natural images from [49]. ↑ means higher values represent better performance and ↓ means lower values represent better performance

Image	Bustince [19]	Wang [50]	M1 [51]	M2 [15]	M3 [52]	Proposed
SA↑	0.8215	0.8281	0.8312	0.8441	0.8494	0.8801
GCE ↓	0.3314	0.3125	0.3035	0.2491	0.2027	0.1980
RI ↑	0.8321	0.8381	0.8427	0.8523	0.8531	0.8824
FE ↑	0.8011	0.8312	0.8401	0.8517	0.8549	0.9089

3.2.3. Results on Kaggle nuclei image

The proposed method was applied to the nuclei images from the Kaggle 2018 dataset. The dataset contained a variety of biological images. Here, the nuclei images were derived from several living beings like humans, mice, and flies. The images were taken in different conditions, like fluorescent and varying illuminations, etc. The uncertainties in the image patterns were high, as evident from the visual inspection of the images shown in Figure 6. The qualitative results of the proposed method are shown in the figure. Different test images from the Kaggle 2018 dataset are shown in row 1 of the figure. The segmentation results by the proposed method are shown in row 2.

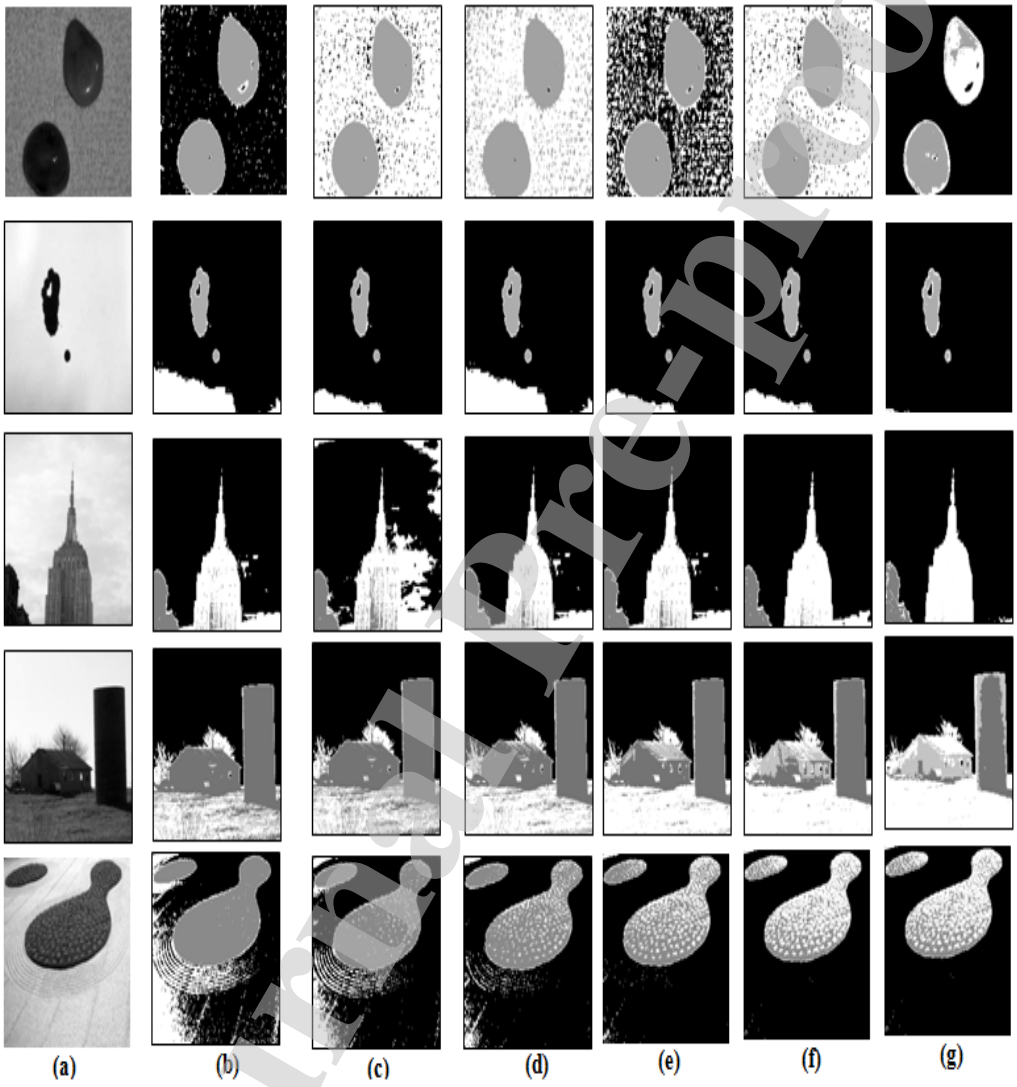

Figure 5: Column wise (a) Original outdoor scene test image.(b) Segmentation by Bustince [19]. (c) Segmentation by Wang [50].(d) Segmentation by method M1 [51].(e) Segmentation by method M2 [15]. (f) Segmentation by the method M3 [52] (g) Segmentation by the proposed method.

The different colors indicate different segments in the images. Visually, it is evident that the proposed method could segment the images properly. If the continuities in the values were considerably low due to the presence of true boundaries, the energy was the lowest with the violation of the constraints and the thresholds were detected. Of course, the penalty came into play with the localization of boundaries. It is to be noted that the number of classes was not known a priori in the proposed method. The average quantitative performance of the proposed method and all the other methods mentioned here are shown in Table 2. From the performances, it is clear that the proposed method could localize the segmentation boundaries accurately with proper segmentation of the classes. It is to be mentioned here that all the other methods mentioned here, had prior knowledge of the number of classes in the images.

Table 2: Quantitative performance of different methods on the images from Kaggle dataset [48]. ↑ means higher values represent better performance and ↓ means lower values represent better performance.

Image	Bustince [19]	Wang [50]	M1 [51]	M2 [15]	M3 [52]	Proposed
SA↑	0.7014	0.8832	0.8834	0.8840	0.8914	0.9001
GCE ↓	0.3902	0.3271	0.3265	0.3012	0.2771	0.1890
RI ↑	0.7133	0.9011	0.9061	0.9121	0.9172	0.9426
FE ↑	0.7802	0.8001	0.8214	0.8355	0.8612	0.9000

3.2.4. Results under different perturbations

In this subsection, we examined the robustness of the different methods under noisy and blurred images. For this purpose, we utilized the NDT images. Two sample test images are shown in Figure 7. The corresponding qualitative results under the different perturbations on the test images are shown in Figure 8. The SAs of the different methods under blurring are shown

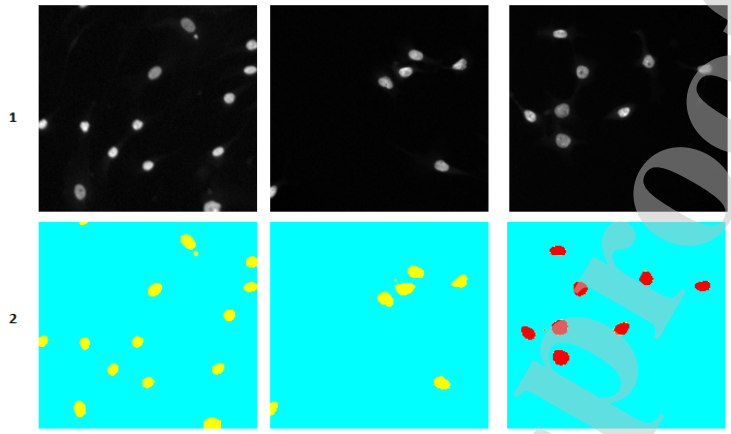

Figure 6: Row wise (1) Original nuclei test images (2) Results using proposed method. Different colors are used to indicate different segments.

in Table 3. From the results, it can be seen that the proposed method is quite robust under a moderate amount of perturbations. The reason may be that under the different perturbations both gray level and spatial ambiguity increase. In the proposed method, the NS helped to reduce the ambiguities by incorporating the weak continuity constraints. In the next subsection, we will examine the performance bound of the methods under noise corruption.

Table 3: The SA of different methods on the blurred images by Gaussian filter with different σ values on NDT dataset [47].

σ	Bustince [19]	Wang [50]	M1 [51]	M2 [15]	M3 [52]	Proposed
$\sigma = 4$	0.7215	0.7422	0.7624	0.7732	0.7843	0.8010
$\sigma = 6$	0.6092	0.7471	0.7542	0.7589	0.7654	0.7940

3.2.5. Statistical validation by modified Cramer-Rao bound

It is already mentioned in Section 3.1 that the performance of the unsupervised segmentation algorithm may vary depending upon the image in hand. So, it is logical to mention the performance bound of a method on a particular image. The performances of the proposed method under different

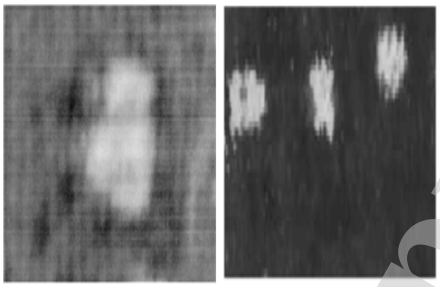

Figure 7: NDT test images for experiments with perturbations.

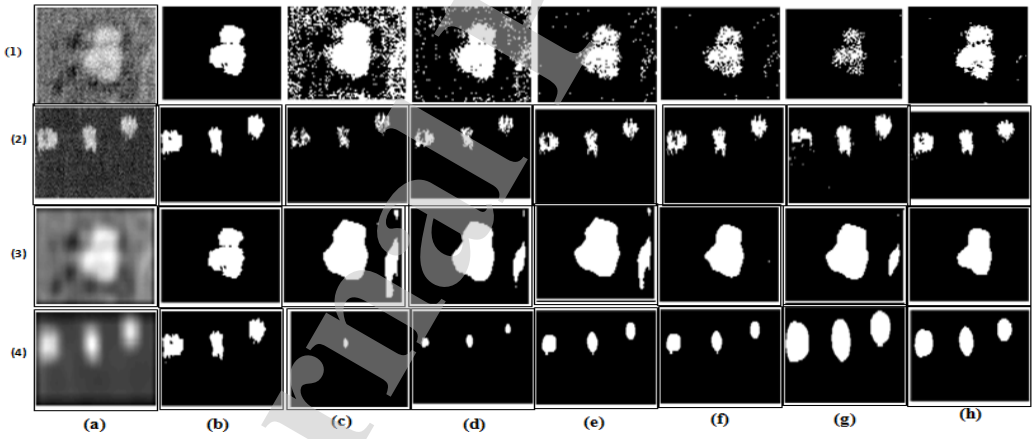

Figure 8: Segmentation results on the images corrupted noise and blurring. Column-wise (a) Row (1) and Row (2): Test images with Gaussian noise of mean 0 and std 0.16. Row (3) and Row (4): Test image blurred by Gaussian filter($\sigma = 4$). (b) Ground truth. (c) Segmentation by Bustince [19].(d) Segmentation by Wang [50](e) Segmentation by method M1 [51].(f) Segmentation by method M2 [15]. (g) Segmentation by the method M3 [52].(h) Segmentation by the proposed method.

Gaussian noises are shown in Figure 9. To statistically bound the performance of the proposed method and all other methods mentioned here we used the modified Cramer-Rao bound(mCRB). The robustness of the methods under the different amounts of corruptions by noise can be mentioned using the bound. For this, we measured the MSE of the segmentation results under different amounts of noise and the lower bound of mCRB for MSE using the method by Peng [45]. We used the measure on the Kaggle 2018 dataset and found out the average performances. To estimate the lower bound the basic non-overlapping regions of the images were taken from the ground truth provided in the dataset. The B-spline function used in the technique was cubic B-spline and the knots were taken after 8 pixels in both horizontal and vertical directions. White Gaussian noise was added with a variance of σ^2 and the performances were measured for the methods under the noise corruption. One sample test image, lower mCRB, and the performances of different methods under different noise perturbations are shown in Figure 10. The dotted line in the graph of Figure 10(b) indicates the minimum MSE that can be achieved by a segmentation method at different SNR on the image in Figure 10(a). The other lines represent the MSE achieved by the different methods on the image. The average MSEs by the methods and the lower bound of MSE on the Kaggle dataset is shown in Figure 11. From the results, it is seen that the proposed method performed satisfactorily in terms of lower MSE compared to other methods. The proposed method was followed by method M3 in terms of statistical performance. The reason for the robustness of the proposed method is as follows. In the proposed method, the weak continuity constraints in the NS domain helped to local-

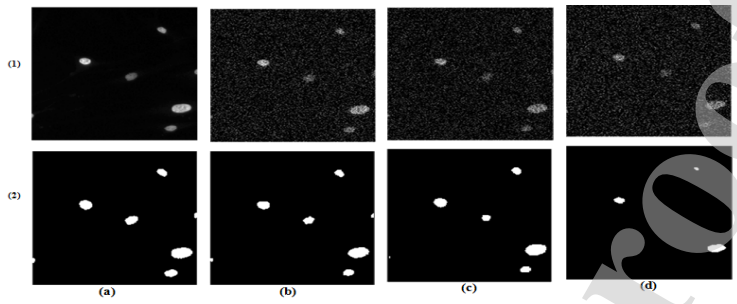

Figure 9: Results by the proposed method on Kaggle images under different Gaussian noise corruption. Column-wise (a) Row(1): Test image. Row (2): Ground truth. (b) Row (1):Test image with Gaussian noise of mean 0 and std 0.09 Row (2): Segmentation by the proposed method. (c) Row (1):Test image with Gaussian noise of mean 0 and std 0.19 Row (2): Segmentation by the proposed method. (d) Row (1):Test image with Gaussian noise of mean 0 and std 0.24 Row (2): Segmentation by the proposed method.

ize the boundaries even in noise corruption. In determining the boundaries, the uncertainties were not increased. On the contrary, due to the lack of boundary information and the inability to localize the boundaries properly, the other methods can not reduce the uncertainties properly.

3.2.6. Comparisons with type-1 fuzzy and type-2 fuzzy set (FS) based uncertainty handling tools

In this subsection, we compared the concept of weak continuity constraints with type-1 [21] and type-2 fuzzy set [24] based uncertainty handling tools with the NS-based approach. We applied the method on Kaggle dataset[48]. The results are shown in Table 4. From, the table it is clear that NS in combination with weak continuity constraints is better than that of type-1 fuzzy set. On the other hand, in terms of qualitative measure type-2 fuzzy set in combination with weak continuity constraints is better than that of the neutrosophic set. But, the main limitation of the type-2 based approach is its type reduction bottleneck. The standard Karnik-Mendel tech-

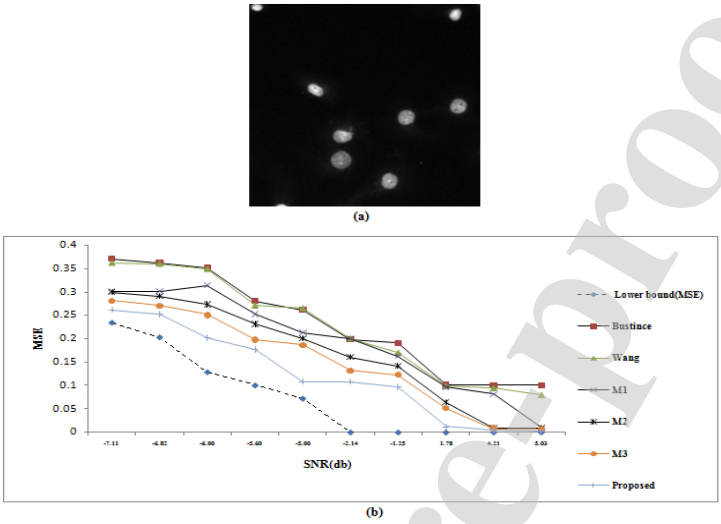

Figure 10: (a) Original test image. (b)Lower bound of MSE and performance by different methods on the image.

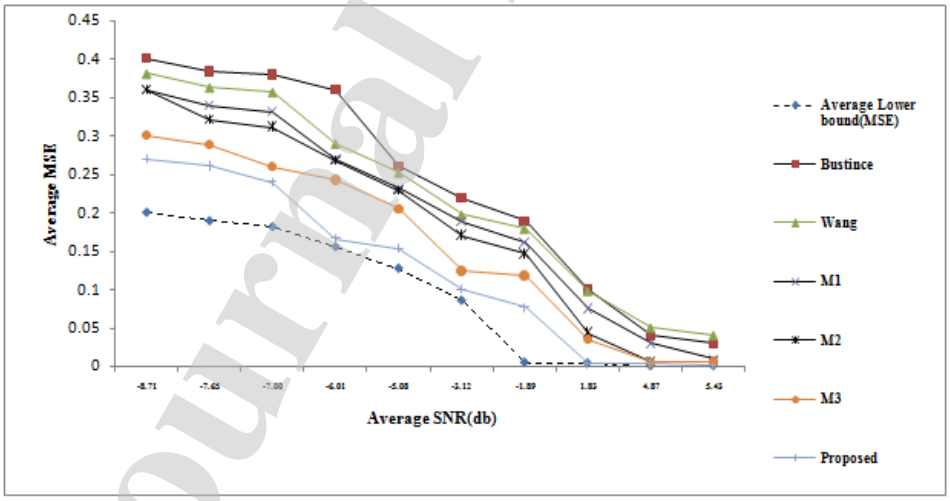

Figure 11: Lower modified Cramer-Rao bound for MSE and performances of different methods under noise corruption.

nique [53] for type reduction is costly. The reason is that a type-2 fuzzy membership function contains an infinite number of embedded type-1 fuzzy membership functions. For accurate type reduction of N sample points, there are requirements of $N-1$ t-norm operations, N multiplications, and $2(N-1)$ division operations. Research is going on to reduce computational complexity [54]. But, no such costly operations are required for a neutrosophic set. So, it is up to the user whether he/she requires high accuracy with high computational complexity or he/she requires good accuracy with low computational complexity.

Table 4: Quantitative comparisons of weak continuity constraints with type-1 FS, type-2 FS and neutrosophic set on Kaggle dataset [48].

Image	type-1 FS [21]	type-2 [24] FS	Neutrosophic set (Proposed)
SA↑	0.8140	0.9213	0.9001
GCE ↓	0.3241	0.1761	0.1890
RI ↑	0.8120	0.9841	0.9426
FE ↑	0.8245	0.9184	0.9000

3.2.7. Speed versus accuracy comparison of the proposed method with other uncertainty handling methods

In a scientific experiment, speed and accuracy are the two important features of performance. In the previous subsection, we tested the performance of the proposed method using different measures. The measures did not take into account the proposed method's speed, i.e. its run time. Here, we used the rate correct score (RCS) [55] to compare the performance of the proposed method to the other methods. The measure takes into consideration the accuracy as well as the speed of a method. The RCS is given by

$$RCS = \frac{v}{\sum RT} \tag{17}$$

Where RT is the response time and v is the number of correct responses. A higher RCS means better performance of a method. In this paper, we considered RT as the run time of the methods compared here. The correct responses were considered based on segmentation accuracy SA. If the segmentation accuracy was more than 0.95, then the response was considered as a correct response. The score of RCS indicates the number of correct results obtained per second. The Kaggle 2018, Weizmann, and NDT image datasets were used for the comparisons. We compared the proposed method with a type-2 based uncertainty handling model in [24] and the conventional type-1 based system proposed in the paper [21]. As already stated in the previous section, both the type-1 FS and type-2 FS-based systems incorporated the concept of weak continuity for multi-class image segmentation. The results are shown in Table 5. All the methods were run using MATLAB 2014 with 8GB RAM.

From the results, it is clear that the NS-based proposed method gave

Table 5: Performance measure of the different methods by RCS. The RCS indicate the number of the correct results obtained per second.

Image dataset	type-1 FS [21]	type-2 FS [24]	Neutrosophic set (Proposed method)
NDT image [47]	0.128	0.189	0.210
Weizmann [49]	0.132	0.184	0.202
Kaggle 2018 [48]	0.129	0.180	0.192

the best performances in terms of RCS compared to both the type-1 FS and type-2 FS-based uncertainty handling models. The reason may be that the run time of the method [24] is high compared to the proposed method due to the interval nature of the type-2 FS. On the other hand, the NS based proposed method can handle the uncertainties better than the type-1 FS based method described in [21].

4. Conclusions and future works

Management of uncertainties in an image pattern is one of the major problems in image segmentation. The current measures of uncertainties do not take into account the boundary information. In this paper, we have proposed an NS-based multi-class segmentation technique in combination with the theory of weak continuity constraints. The weak continuity constraints take care of the boundary information and help to localize the segmentation boundaries accurately. By doing this, the gray level and spatial ambiguities are decreased in the segmentation process. The energy function in the NS domain acts as an objective function in the segmentation process. We have shown that the minimization of the objective function minimizes the gray and spatial level ambiguities. The proposed technique helps to overcome the limitation of current techniques for image segmentation in the NS domain by taking into consideration the localization of segment boundaries. In the proposed method, the accurate thresholds values are determined iteratively by minimizing the energy function without any prior knowledge about the number of classes. The iteration produces a tree structure for the segmentation process. The iteration stops depending on a stopping criterion called the segmentation index. The technique is advantageous in situations when the number of classes is not available.

The method performed quite well on the synthetic and variety of natural and NDT images. The images contain highly uncertain image patterns as evident from their histograms. The method performs better both quantitatively and qualitatively than that of the other methods compared here. Also, the performance of the proposed method on the highly uncertain Kaggle nuclei

images is better than that of the state-of-the-art methods. The robustness of the proposed method under the noise perturbations is satisfactory and it is verified statistically by modified Cramer-Rao bound.

The proposed method is an iterative process for segmentation and hence slower than a non-iterative process. Future research may be directed towards the speed up of the iterative process to make it time-efficient. The proposed technique can also be applied to a rough set, which is also a powerful tool for uncertainty reduction in the segmentation process. We are currently investigating the technique to apply the weak string energy concept in the rough set domain. The scope for future research is also to apply the sting theory to complex textured images.

5. References

[1] S. S. Martínez, C. O. Vázquez, J. G. García, J. G. Ortega, Quality inspection of machined metal parts using an image fusion technique, Measurement 111 (2017) 374–383.

[2] N. Razmjooy, V. V. Estrela, Applications of image processing and soft computing systems in agriculture, IGI Global, 2019.

[3] P. R. G. Kurka, A. A. D. Salazar, Applications of image processing in robotics and instrumentation, Mechanical Systems and Signal Processing 124 (2019) 142–169.

[4] G. Dougherty, Digital image processing for medical applications, Cambridge University Press, 2009.

[5] A. Radu, M. Carmen, Industrial applications of image processing, Acta Universitatis Cibiniensis 1 (64) (2014) 17–21.

[6] J. F. Canny, Finding edges and lines in images., Tech. rep., Massachusetts Institure Of Technology Cambridge Artificial Intelligence Lab (1983).

[7] S. K. Pal, A. Ghosh, B. U. Shankar, Segmentation of remotely sensed images with fuzzy thresholding, and quantitative evaluation, International Journal of Remote Sensing 21 (11) (2000) 2269–2300.

[8] Z. Zhang, F. Xing, H. Wang, Y. Yan, Y. Huang, X. Shi, L. Yang, Revisiting graph construction for fast image segmentation, Pattern Recognition 78 (2018) 344–357.

[9] J. Bragantini, S. B. Martins, C. Castelo-Fernandez, A. X. Falcão, Graph-based image segmentation using dynamic trees, in: Iberoamerican Congress on Pattern Recognition, Springer, 2018, pp. 470–478.

[10] E. Z. Mequanint, L. T. Alemu, M. Pelillo, Dominant sets for constrained image segmentation, IEEE Transactions on Pattern Analysis and Machine Intelligence 41 (10) (2019) 2438–2451.

[11] S. Niu, Q. Chen, L. De Sisternes, Z. Ji, Z. Zhou, D. L. Rubin, Robust noise region-based active contour model via local similarity factor for image segmentation, Pattern Recognition 61 (2017) 104–119.

[12] K. Ding, L. Xiao, G. Weng, Active contours driven by local pre-fitting energy for fast image segmentation, Pattern Recognition Letters 104 (2018) 29–36.

[13] K. Zhang, H. Song, L. Zhang, Active contours driven by local image fitting energy, Pattern recognition 43 (4) (2010) 1199–1206.

[14] S. Borjigin, P. K. Sahoo, Color image segmentation based on multi-level tsallis–havrda–charvát entropy and 2d histogram using pso algorithms, Pattern Recognition 92 (2019) 107–118.

[15] P. Upadhyay, J. K. Chhabra, Kapurs entropy based optimal multilevel image segmentation using crow search algorithm, Applied Soft Computing (2019) 105522.

[16] R. Assaf, A. Goupil, V. Vrabie, T. Boudier, M. Kacim, Persistent homology for object segmentation in multidimensional grayscale images, Pattern Recognition Letters 112 (2018) 277–284.

[17] Y. Wang, R. Zeng, Image segmentation algorithm based on geometric flow bandelets transformation particle replanting, Pattern Recognition Letters 116 (2018) 200–204.

[18] T. Lei, X. Jia, Y. Zhang, L. He, H. Meng, A. K. Nandi, Significantly fast and robust fuzzy c-means clustering algorithm based on morphological reconstruction and membership filtering, IEEE Transactions on Fuzzy Systems 26 (5) (2018) 3027–3041.

[19] H. Bustince, E. Barrenechea, M. Pagola., Image thresholding using restricted equivalence function and minimizing the measures of similarity., Fuzzy Sets and Systems. 158 (2007) 496–516.

[20] P. Maji, M. K. Kundu, B. Chanda, Second order fuzzy measure and

740 weighted co-occurrence matrix for segmentation of brain mr images,
741 Fundamenta Informaticae 88 (1-2) (2008) 161–176.

742 [21] S. Dhar, M. K. Kundu, Multi-class image segmentation using theory
743 of weak string energy and fuzzy set, in: Intelligence Enabled Research,
744 Springer, 2020, pp. 33–40.

745 [22] P. Roy, S. Goswami, S. Chakraborty, A. T. Azar, N. Dey, Image segmen-
746 tation using rough set theory: a review, International Journal of Rough
747 Sets and Data Analysis (IJRSDA) 1 (2) (2014) 62–74.

748 [23] F. Smarandache, A Unifying Field in Logic,Neutrosophy, Neutrosophic
749 Set,Neutrosophic Probability, 3rd Edition, American Research Press,
750 2003.

751 [24] S. Dhar, M. K. Kundu, Interval type-2 fuzzy set and theory of weak
752 continuity constraints for accurate multiclass image segmentation, IEEE
753 Transactions on Fuzzy Systems 28 (9) (2019) 2151–2163.

754 [25] Y. Guo, Y. Akbulut, A. Şengür, R. Xia, F. Smarandache, An efficient
755 image segmentation algorithm using neutrosophic graph cut, Symmetry
756 9 (9) (2017) 185.

757 [26] Y. Guo, A. Şengür, A novel image segmentation algorithm based on
758 neutrosophic similarity clustering, Applied Soft Computing 25 (2014)
759 391–398.

760 [27] L. Li, L. Sun, Y. Xue, S. Li, X. Huang, R. F. Mansour, Fuzzy multilevel
761 image thresholding based on improved coyote optimization algorithm,
762 IEEE Access 9 (2021) 33595–33607.

[28] A. Wunnava, M. K. Naik, R. Panda, B. Jena, A. Abraham, An adaptive harris hawks optimization technique for two dimensional grey gradient based multilevel image thresholding, Applied Soft Computing 95 (2020) 106526.

[29] A. Raj, G. Gautam, S. N. H. S. Abdullah, A. S. Zaini, S. Mukhopadhyay, Multi-level thresholding based on differential evolution and tsallis fuzzy entropy, Image and Vision Computing 91 (2019) 103792.

[30] K. Sowjanya, S. K. Injeti, Investigation of butterfly optimization and gases brownian motion optimization algorithms for optimal multilevel image thresholding, Expert Systems with Applications (2021) 115286.

[31] S. Dhar, M. K. Kundu, A novel method for image thresholding using interval type-2 fuzzy set and bat algorithm, Applied Soft Computing 63 (2018) 154–166.

[32] C. Liu, W. Liu, W. Xing, An improved edge-based level set method combining local regional fitting information for noisy image segmentation, Signal Processing 130 (2017) 12–21.

[33] A. Blake, A. Zisserman, Weak continuity constraints in computer vision., Tech. rep., University of Edinburgh (1986).

[34] A. Blake, A. Zisserman, Visual reconstruction, MIT press, 1987.

[35] H. Cheng, Y. G. and, A new neutrosophic approch to image segmentation, Pattren Recognition . 42 (2009.) 587–595.

[36] H. Cheng, Y. Guo, A new neutrosophic approch to image thresholding, New Mathematics and Natural Computation. 4 (3) (2008.) 291–308.

[37] H. Cheng, Y. Guo, Y. Zhang, A novel image segmentation approach based on neutrosophic set and improved fuzzy c-means algorithm, New Mathematics and Natural Computation 7 (01) (2011) 155–171.

[38] S. Dhar, M. K. Kundu, Accurate segmentation of complex document image using digital shearlet transform with neutrosophic set as uncertainty handling tool, Applied Soft Computing 61 (2017) 412–426.

[39] A. Sengur, Y. Guo, Color texure segmentation based on neutrosophic set and wavelet transform, Computer Vision and Image Understanding. 115 (2011.) 1134–1144.

[40] M. Acharyya, R. K. De, M. K. Kundu, Extraction of features using m-band wavelet packet frame and their neuro-fuzzy evaluation for multitexture segmentation, IEEE Transactions on Pattern Analysis and Machine Intelligence 25 (12) (2003) 1639–1644.

[41] C. Li, R. Huang, Z. Ding, J. C. Gatenby, D. N.Metaxas, J. C. Gore., A level set method for image segmentation in the presence of intensity inhomogeneitics with application to MRI., IEEE Transactions on Image processing. 20 (7) (2011) 2007–2016.

[42] K. Al-Dulaimi, I. Tomeo-Reyes, J. Banks, V. Chandran, White blood cell nuclei segmentation using level set methods and geometric active contours, in: 2016 International Conference on Digital Image Computing: Techniques and Applications (DICTA), IEEE, 2016, pp. 1–7.

[43] B. Ziółko, D. Emms, M. Ziółko, Fuzzy evaluations of image segmentations, IEEE Transactions on Fuzzy Systems 26 (4) (2018) 1789–1799.

[44] Y. Zhang., A survey on evaluation methods for image segmentation. image segmentation evaluation: A survey of unsupervised methods., Pattern Recognition. 29 (1996) 1335–1346.

[45] R. Peng, P. Varshney, On performance limit of image segmentation algorithms, Computer Vision and Image understanding 132 (2015) 24–38.

[46] https://commons.wikimedia.org/wiki/Category:Images.

[47] M. Sezgin, B. Sankur, Survey over image thresholding techniques and quantitative performance evaluation., Journal of Electronic Imaging 13 (1) (2004) 146–165.

[48] http://data.broadinstitute.org/bbbc/BBBC038/.

[49] S. Alpert, M. Galun, A. Brandt, R. Basri, Image segmentation by probabilistic bottom-up aggregation and cue integration, IEEE transactions on pattern analysis and machine intelligence 34 (2) (2011) 315–327.

[50] D. Wang, H. Li, X. Wei, X.-P. Wang, An efficient iterative thresholding method for image segmentation, Journal of Computational Physics 350 (2017) 657–667.

[51] Y. Guo, A. Sengur, Ncm: Neutrosophic c-means clustering algorithm, Pattern Recognition 48 (8) (2015) 2710–2724.

[52] S. Jha, R. Kumar, I. Priyadarshini, F. Smarandache, H. V. Long, et al., Neutrosophic image segmentation with dice coefficients, Measurement 134 (2019) 762–772.

[53] N. N. Karnik, J. M. Mendel, Centroid of a type-2 fuzzy set, information Sciences 132 (1-4) (2001) 195–220.

[54] Y. Chen, Study on centroid type-reduction of interval type-2 fuzzy logic systems based on noniterative algorithms, Complexity 2019.

[55] A. Vandierendonck, A comparison of methods to combine speed and accuracy measures of performance: A rejoinder on the binning procedure, Behavior research methods 49 (2) (2017) 653–673.

Highlights

- **The method segments an image using the concept of weak continuity constraints.**
- **The constraints in neutrosophic domain help to manage uncertainties.**
- **The method automatically segments an image without prior knowledge about the number of classes.**

CRediT author statement

Soumyadip Dhar: Methodology, Writing-Review and Editing.

Malay K. Kundu: Conceptualization, Supervision

Declaration of interests

☐The authors declare that they have no known competing financialinterestsor personal relationships that could have appeared to influence the work reported in this paper.

☐The authors declare the following financial interests/personal relationships which may be considered as potential competing interests:

Declarations of interest: ‘none'